Published in final edited form as:

Anal Chem. 2019 December 03; 91(23): 15032–15039. doi:10.1021/acs.analchem.9b03709.

Flow-encoded oxygen control to track the time-dependence of molecular changes induced by static or cycling hypoxia.

Ming Yao[†], **Zahid N. Rabbani**[‡], **Tyler Sattler**[‡], **Khue G. Nguyen**[‡], **David A. Zaharoff**[‡], **Glenn Walker**[‡,§], **Michael P. Gamcsik**[‡,*]

[†]Department of Mechanical & Aerospace Engineering, North Carolina State University, Raleigh, North Carolina 27695

[‡]UNC/NCSU Joint Department of Biomedical Engineering, Raleigh, North Carolina 27695

Abstract

Detecting the effects of low oxygen on cell function is often dependent on monitoring the expression of a number of hypoxia markers. The time dependence of the appearance and stability of these markers varies between cell lines. Assessing cellular marker dynamics is also critical to determining how quickly cells respond to transient changes in oxygen levels that occurs with cycling hypoxia. We fabricated a manifold designed to use flow-encoding to produce sequential changes in gas mixtures delivered to a permeable-bottom 96-well plate. We show how this manifold and plate design can be used to expose cells to either static or cycling hypoxic conditions for eight different time periods thereby facilitating the study of the time-response of cells to altered oxygen environments. Using this device, we monitored the time-dependence of molecular changes in human PANC-1 pancreatic carcinoma and Caco-2 colon adenocarcinoma cells exposed to increasing periods of static or cycling hypoxia. Using immunohistochemistry, both cell lines show detectable levels of the marker protein hypoxia-inducible factor-1α (HIF-1α) after 3 h of exposure to static hypoxia. Cycling hypoxia increased the expression level of HIF-1α compared to static hypoxia. Both static and cycling hypoxia also increased glucose uptake and aldehyde dehydrogenase activity. This new device offers a facile screening approach to determine the kinetics of cellular alterations under varying oxygen conditions.

Graphical Abstract

[*]**Corresponding Author:** mgamcsi@ncsu.edu, Phone: 919-513-0786.

[§]Present Addresses

Department of Biomedical Engineering, University of Mississippi, Oxford, Mississippi 38677

Author Contributions

The manuscript was written through contributions of all authors. All authors have approved the final version of the manuscript.

The authors declare no competing financial interests.

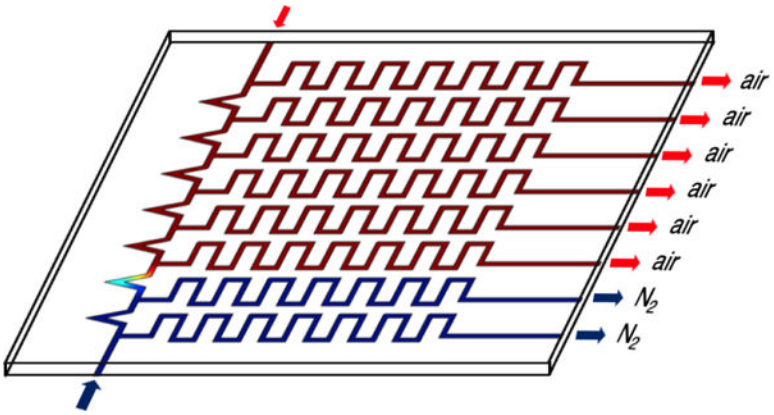

Defining the molecular characteristics of hypoxic tumor tissue *in vivo* is challenging as tissue hypoxia varies spatially and temporally.[1] *In vitro* models offer the capability to systematically control both the level of static hypoxia and the amplitude and periodicity of cycled oxygen levels. However, typical *in vitro* experiments may probe only a few levels of static hypoxia or a few cycles of intermittent hypoxia that represent only a small fraction of the oxygen environments present in the *in vivo* tumor. We have shown that a permeable-bottom multiwell plate attached to a custom-fabricated gas mixer and delivery manifold can be used to probe a far greater number of static or cycling hypoxic conditions.[2] This device demonstrated that, in Caco-2 cells, the hypoxia marker hypoxia-inducible factor-1α (HIF-1α) was detectable by immunohistochemistry after 24 h of exposure to oxygen partial pressure (pO_2) levels between 1 – 37 mmHg. However, many reports indicate that HIF-1α protein levels vary with time[3–13] and that HIF-1α mRNA[5] level and transcriptional activity do not correlate with protein levels.[6] The time course of HIF-1α activity influences transcription of downstream genes for the glucose transporter-1 (GLUT-1)[14] and also controls factors that promote stem cell-like behavior that is often detected by an increase in aldehyde dehydrogenase (ALDH) activity.[15] Therefore, it is important to assess the time dependence of the appearance and stability of molecular makers in any study in which cells are exposed to changing oxygen conditions. In addition, the rate of change of molecular components will also affect how cells respond to cyclical changes in oxygen content that occur in tumor tissue.

In order to facilitate time course studies, we have modified our earlier manifold design[2] to sequentially expose each row of a 96-well plate to different periods of hypoxia. This device offers several advantages to other approaches: (*i*) Permeable-bottom plate design delivers known, uniform gas mixtures to cells. (*ii*) Low gas consumption compared to hypoxia chambers, cabinets or incubators. (*iii*) Allows rapid switching to mimic cycling hypoxia profiles found *in vivo* compared to the time it takes to flush/equilibrate hypoxia chambers and conventional plates. (*iv*) Flow-encoded switching precludes the need for multiple gas delivery systems and/or chambers. (*v*) Final readouts for multiple time points are performed on one plate thereby reducing variations in conditions using different plates. (*vi*) Multiple cell lines or molecular assays can be performed on one plate. (*vii*) Unlike microfluidic devices, this plate can be used with conventional multichannel pipettors and plate readers.

We used this device to expose PANC-1 and Caco-2 cells to timed intervals of both static and cycling hypoxia. We show that upon exposure to static hypoxia, HIF-1α levels are first detected by immunohistochemistry after 3 h of exposure and steadily increase over 24 h. Cycling, as opposed to static hypoxia, leads to higher levels of HIF-1α staining detected after 24 h in both cell lines. Both static and cycling hypoxia lead to steadily increasing glucose uptake activity over 24 h that was detected by an increased uptake of the fluorescent probe analog 2-deoxy-2-((7-nitro-2,1,3-benzoxadiazol-4-yl)amino)-D-glucose (2-NBDG). Similarly, steadily increasing ALDH activity was detected over 24 h of static hypoxia using the fluorescent probe boron-dipyrromethene-aminoacetaldehyde (BAAA, ALDEFLUOR™). This study demonstrates how a single multiwell plate can be used to detect the time course of molecular and functional activity changes in cells exposed to static or cycling hypoxia.

MATERIALS AND METHODS

Cell Culture.

The human cell line, PANC-1 pancreatic adenocarcinoma and Caco-2 colon adenocarcinoma were purchased from the American Type Culture Collection (Manassas, VA) and grown in high glucose containing Dulbecco's Modified Eagle's Medium (Gibco), with 10% fetal bovine serum (Gibco) without antibiotics. Cells were seeded to minimize the 'edge effect' often seen in 96-well plates.[2] Cells were cultured for 24 h under air/CO_2 atmospheres before placement in the gas manifold for hypoxia experiments.

Device Fabrication.

The gas channels and manifold were fabricated from polymethylmethacrylate (acrylic) polymer sheets and the gasket from Buna-N rubber as described previously.[2] The manifold pattern is etched onto one acrylic plate and heat-bonded to another plate to provide a gas-tight seal. Membranes were spin cast using polydimethylsiloxane (PDMS) polymer (Sylgard 184) to yield membranes of 125 μm thickness. Bottomless 96-well plate (Greiner Bio-One) were treated with 1% v/v solution of (3-aminopropyl)triethoxysilane (Sigma) in water for 15 min to adhere the PDMS membrane. The fabricated PDMS membranes were coated with fibronectin as described previously.[2]

Immunohistochemistry.

Adherent cells were fixed with 4% paraformaldehyde in phosphate buffered saline for 15 minutes, washed with saline, permeabilized with 0.1% Triton X-100 and rinsed with saline. The cells were incubated overnight with primary antibodies HIF-1α (1:200, Thermo Fisher, catalog #MA1–516) followed by DyLight 488, goat anti-mouse IgG (1:400), (Thermo Fisher, catalog #35502). After washing with saline, cells were counterstained with 4',6-diamidino-2-phenylindole (DAPI). Microscopy was performed on an Olympus IX-71 inverted epifluorescence microscope with an ORCA-ER cooled monochrome charge-coupled device camera.

Glucose Uptake Activity.

Media was removed and the cells were washed three times with PBS. 100μL of glucose-free cell media containing 150μM 2-NBDG (Cayman Chemical) was added to each well, and the

plate was incubated at 37°C for 35 mins. The reaction was stopped by adding cold PBS. After washing with three-times with ice-cold PBS, cells were imaged by fluorescence microscopy.

Cell Counting and Image Analysis.

Well plates were seeded with 1.5 x 10^4 cells/well and allowed to attach for 24 h under normoxic incubator conditions. Then N_2/CO_2 was introduced into the manifold to provide static hypoxic conditions for periods ranging between 1 and 24 h. For counting, nuclei were stained with DAPI and imaged using fluorescence microscopy. Nuclei in an image field were delineated and enumerated using NIH ImageJ software.[16] For quantification of HIF-1α staining and 2-NBDG uptake, the total integrated fluorescence intensity in the field of cells was determined using ImageJ by the procedure of McCloy et al.[17] Each data point shown was the average fluorescence intensity (± one standard deviation (SD)) for 3 different wells at each timepoint. The statistical significance of the data was calculated using Students t-test in Microsoft Excel.

Cell Viability.

Cell viability was measured using the Promega CellTiter-Glo bioluminescence assay in PDMS-bottom plates and a BioTek Cytation plate reader.

ALDH Activity.

Media was removed and the cells were washed three times with PBS. 100μl of ALDEFLUOR™ Assay Buffer (Stem Cell Technologies, Inc.) containing 5μl/mL of BAAA Reagent was added to each well and the plate was incubated at 37°C for 40 mins. The reaction was stopped by adding cold PBS and washed three-times with ice-cold PBS. To slow cellular efflux of the fluorescent product of the ALDH reaction, we filled the troughs surrounding individual wells on the Greiner Bio-One plates with ice-cold PBS to keep the plates cool during microscopy.

Flow Cytometry.

The ALDH activity was measured using the ALDEFLUOR™ assay kit according to the manufacturer's instructions. 30,000 cells were seeded in each well of the 96 well plate and cultured in the manifold. Cells were trypsinized, washed with pre-warmed assay buffer and incubated with reagent for 40 min at 37°C in the presence or absence of the inhibitor N,N-diethylaminobenzaldehyde (DEAB). Following incubation, data were acquired using a BD FACSCelesta flow cytometer (BD Biosciences) and analyzed using FlowJo software (Tree Star, Ashland, OR).

Oxygen Sensing.

Oxygen measurements in gas mixtures, water and cell growth media were obtained from fiber optic sensors housed within a protective syringe needle (Profiling Oxygen Microsensor, PreSens, Germany). PreSens specifications indicate a sensitivity down to pO_2 = 0.4 mmHg.[18] Oxygen partial pressure (pO_2) is used to express gas and liquid oxygen content in our devices. Sensors were calibrated each day by a two-point calibration method for gas or

liquid readings.[2] For readings in the wells, we translated the fiber tip to a point 100 μm short of the needle tip to prevent breakage as the tip rested on the membrane surface. The fiber tip was exposed to the environment but remained within the protective needle bevel. Because the fiber optic was recessed, the sensor provided readings 100 μm above the membrane.[2] This partially retracted position did not affect readings.

Gas Flow Control.

Gas supplied to culture plates was delivered by mass flow controllers (Aalborg) directed by LabView-based software (National Instruments). All experiments used two feed gas mixtures for delivery to the plate mixing tree and manifold: Gas Input 1: 95% N_2/5% CO_2, and Gas Input 2: 95% air/5% CO_2. Hereafter, for convenience, these gas mixtures will be referred to as N_2/CO_2 and air/CO_2, respectively. Gas flow rates were changed at different time points with a LabView program.

Theoretical Modeling.

The designs of the gas channels, manifold and 96-well plates were evaluated by modeling the theoretical gas transfer capabilities of each design by finite element analysis using COMSOL Multiphysics® software. In COMSOL, the “Transport of Diluted Species” and “Laminar Flow” toolboxes were used to create 2D models of oxygen transport in the gas channels, manifold and plate. The oxygen diffusion coefficients through culture media and the 125 μm thick PDMS membrane are given in our earlier publication.[2] For predicting the impact of cellular oxygen consumption on gas mixture content, a row of 12 wells were modeled with gas flow beneath the row. Each well in the row was ‘filled’ with 50,000 cells consuming oxygen at a rate of 3.5×10^{-17} mol $O_2 \cdot cell^{-1} \cdot s^{-1}$.[19]

RESULTS

Manifold Design Principle.

The principle behind this device is to use a gas manifold to deliver one of two different input gases to gas-tight channels below each row (A-H) of a permeable-bottom 96-well plate. For this study, Input Gas 1 is an anoxic gas mixture consisting of N_2/CO_2 and Input Gas 2 is a high oxygen content gas mixture, air/CO_2. In all of the studies reported herein, the tops of the wells were not sealed and the media surface in each well equilibrates with the ambient surrounding atmospheric oxygen. In these open wells, an oxygen gradient is generated with the gas content at the well bottom dominated by the gas mixture from below.[2]

Initially (t_0), air/CO_2 is delivered to all wells and then at predetermined time points (t_1-t_7), individual rows are switched to the N_2/CO_2 mixture thereby generating an anoxic atmosphere below the wells in these rows. Rather than relying upon a complex plumbing/switching system to change gas content, we use a simple manifold design shown in Figure 1, combined with gas flow controllers to adjust the flow rates of air/CO_2 and N_2/CO_2 entering the manifold. The relative flow rates of air/CO_2 and N_2/CO_2 determine the number of rows exposed to each gas. For example, if the flow rates are equal, half the rows will be normoxic and the other half anoxic. This “flow-encoded switching” approach has been used to control

liquid delivery to cells in microfluidic devices.[20] Flow rates can be controlled using manual flow meters, or in our case, computer-controlled flow meters.

Computational models of the manifold design.

Flow-encoded switching uses step increases in gas flow rates to sequentially overcome flow resistance in a series of parallel gas channels. Since flow resistance is related to the dimensions of each gas channel, mathematical modeling was used to design a gas manifold that would produce the desired sequential switching pattern. COMSOL software was used to determine the channel dimensions and flow rates which would allow sequential switching of gas outputs to rows A-G on a 96-well plate from Input Gas 1 to Input Gas 2. In these studies, gas output to row H remains as a normoxic control. Since it is easiest to verify our modeling results at room temperature using dry gases, this modeling was used to find conditions that will deliver either dry air/CO_2 (pO_2 = 151 mmHg) or dry N_2/CO_2 (pO_2 = 0 mmHg) at 22 °C. The final design is shown in Figure 1. The channels in this design are 1 mm wide and 1 mm deep. The number of channel meanders are dictated by the need to accommodate a long channel in a small footprint. The design has two input gas ports directing gas flow into a manifold with eight outlet ports. At t_0, flow from Input 1 (N_2/CO_2) is zero and all flow comes through Input 2 (air/CO_2) then all eight output channels will deliver air-CO_2 (pO_2 = 151 mmHg) to outputs to rows A-H (Figure 1). By increasing the flow rate of N_2/CO_2, the gas delivered to each row can sequentially be changed over to the N_2/CO_2 gas mixture. The predicted flow rates needed to switch outputs to rows A and B at time points t_1 and t_2 are given by the numbers above the red and blue arrows in Figure 1 to produce the pO_2 heat maps shown. For brevity, only the flow rates needed to switch the first two channels are shown in Figure 1. The heat maps showing switching of all channels is shown in Figure S1. The predicted flow rates necessary to make the switches to these outputs across all channels are given in Table 1. Table 1 shows that by adjusting gas flow rates, pO_2 levels can be controlled to within 0.6 mmHg of the desired levels of either 0 or 151 mmHg.

The gas pO_2 level delivered to a row of 12 cell-filled wells on a plate will change as the gas flows past each well as oxygen is consumed. COMSOL modeling was used to determine if a flow rate of 3 mL/min will deliver sufficient oxygen to 50,000 cells in each of 12 wells in a row to maintain a uniform gas content. Models predict a decrease in gas pO_2 = 0.01 mmHg when air-CO_2 flows at 3 mL/min from beneath a cell-filled well in Column 1 to a well in Column 12 (Figure S1). This difference would be undetectable by our probes.

Experimentally measured static gas outputs from the manifold.

Based on the design in Figure 1, the gas manifold was fabricated. Initially, the N_2/CO_2 flow was zero through the manifold as shown in the line t_0 in Table 1. Then every five minutes, the flow rates were changed as shown in Table 1 to sequentially change outputs to rows A – G to the N_2/CO_2 gas mixture. Oxygen sensors were used to measure the outputs from each channel over time and these data are shown in Figure 2. The flow controllers used in this study can switch within milliseconds. The oxygen sensors take a reading every second but have a reported response time of <15 s for gas measurements. The first flow-encoded switch is at the lowest flow rate of 3 mL/min. The fastest flow rate in any output is under the conditions designated at timepoint t_4 (Table 1), where both inputs deliver at a rate of 100

mL/min resulting in each of the eight output channels producing flow rates at 25 mL/min. Over this flow range, all outputs produce pO_2 readings <1 mmHg within a minute of switching (data not shown). The final flow rates used at time point t_7 results in the output to row H remaining at 151 mmHg for the entire 40 minutes of readings. The data in Figure 2 indicate that at the end of the timed sequence, the channel output to row A delivered N_2/CO_2 for 35 minutes and outputs to rows B - G delivered this gas mixture for 30, 25, 20, 15, 10 and 5 minutes, respectively.

Experimentally measured cycling gas output from the manifold.

In addition to static gas delivery, the flow controllers can be programmed to produce cycling gas levels for increasing periods of time. For example, based on the flow rates given in Table 1, if the gas flow from Input 1 is switched between 3 mL/min and 19 mL/min periodically, then the gas output to row B will continuously cycle between pO_2 levels of 0 mmHg and 151 mmHg while output A remains at 0 mmHg and C remains at 151 mmHg. Figure 3 shows the measured outputs when this cycling is done every 5 minutes. Under these conditions, outputs D to H remain at 151 mmHg (not shown). Using the flow rates in Table 1, any row can be exposed to timed cycling patterns and in our cell studies, 30 min cycling times were used.

Measured O_2 levels in the wells under static flow.

The manifold was incorporated into a base plate to deliver the gas mixtures to eight channels below each row of a permeable-bottom 96-well plate. A diagram of the device is shown in Figure 4(A) using a 96-well plate with a bottom fabricated from a 125 μm thick film of PDMS. The assembled device is shown in Figure 4(B). We showed in our earlier work that a PDMS membrane is best suited for rapid delivery of gas mixtures to the cells grown on top of this membrane.[2] The plate, gasket and manifold were assembled and the wells filled with 0.300 mL of water for testing. In all experiments, the tops of the wells were exposed to ambient air atmospheres surrounding the plates. When anoxic gas is applied below a row in the plates, this generates an oxygen gradient in the water from high levels at the top surface to anoxic conditions in the channels below the permeable membrane and hypoxic conditions at the membrane surface.

The data in Figure 5 shows the time response of the oxygen sensor immersed in water in a plate well in a humidified air/CO_2 incubator at 37 °C. In this case, the Input Gas 2 is humidified at 37 °C to deliver a pO_2 level of 141 mmHg.[19] The sensor records the pO_2 levels at a point 100 μm above the PDMS upper membrane surface (see Methods section). The time response is different for 3 and 25 mL/min gas flow rates, which have time constants of τ = 0.7 and 0.4 min, respectively. Using 5τ to estimate the time required to attain 99% of the desired gas level suggests that the flow rates could be switched every 3.5 or 2.0 min. The sensor readings equilibrated at a measured pO_2 = 2.2 ± 1.0 mmHg at steady state. Since the PDMS membrane is 125 μm thick, the oxygen level at the top of the membrane, where cells would be growing, is 1.1 mmHg. For three plates fabricated over 1 month, the average (±SD) for measured pO_2 = 1.0 ± 1.1 mmHg when flowing N_2/CO_2 through the device. The large SD is due to the sensors operating near their sensitivity limit.

To demonstrate the resolution in pO_2 control attainable in the device, the inset in Figure 5 shows the sensor readings as the delivered gas is cycled between N_2/CO_2 and 1% air/CO_2; (pO_2 between 0 and 1.6 mmHg), every 5 min at a flow rate of 25 mL/min. These data show we can reliably control and differentiate between pO_2 levels of 2 mmHg.

Screening cellular response to changing oxygen levels.

In order to determine the effect of static hypoxia on cell viability or molecular responses, flow encoding was used to change wells in row A from 140 mmHg to ~1 mmHg at the first time point (t = 0 h). Cells in rows B – G were switched over at t = 6, 12, 15, 18, 21 and 23 h. Row H remained at 137 mmHg. This results in a plate with cells exposed to hypoxia for 24, 18, 12, 9, 6, 3, 1, 0 h periods for rows A – H, respectively. Viabilities or cell numbers were no different between normoxic PANC-1 or Caco-2 cells and cells exposed to 24 h of hypoxia (Figure S2).

For cycling hypoxia, the flow rates of the gases were altered on 30 min cycles (30 min high pO_2 – 30 min low pO_2) for periods of 24, 18, 12, 9, 6, 3 h for cells in rows B – H.

Time course of changes in HIF-1α expression under hypoxia.

The presence of HIF-1α protein in PANC-1 cells was monitored in fixed cells after exposure to 0 – 24 h of hypoxia by immunohistochemistry. The results shown in Figure 6 show little or no HIF-1α detectable in cells exposed to normoxia (0 h) or after 1 h of static hypoxia. Low levels of HIF-1α are detected after 3 h that increased up to 24 h. These data were quantified by image analysis and the results are shown in Figure 7(A). A statistically significant increase in HIF-1α is detected at 3 h that increases up to 24 h.

For the PANC-1 cells exposed to cycling hypoxia, HIF-1α staining was seen at 3 h with levels increasing up to 24 h. Cycling resulted in higher levels of HIF-1α expression compared to static hypoxia. The quantified data is shown in Figure 7(A) with statistically significant increases after 3 h.

Similar results were in the Caco-2 cell line with micrographs shown in Figure S3 and quantification of the images in Figures 7(A). HIF-1α exposed to static hypoxia is significantly increased after 6 h and further increased up to 24 h. When exposed to cycling hypoxia, the Caco-2 line also shows increased HIF-1α staining compared to the static levels, with significant increases as soon as 3 h.

Time course of changes in glucose uptake activity under hypoxia.

The fluorescent glucose analog 2-NBDG is a functional marker of glucose uptake activity *via* one or more of the glucose transporters.[21] The time dependence of 2-NBDG uptake upon exposure to static and cycling hypoxia for both the PANC-1 and Caco-2 cell lines were detected by fluorescence microscopy. The micrographs are shown in Figures S4. Both static and cycling hypoxia induce a steady increase in the uptake of 2-NBDG over 24 h. Cycling hypoxia results in a higher level of 2-NBDG uptake at all time points. The image intensities due to increased uptake of 2-NBDG were quantified and are shown in Figure 7(B). Static hypoxia shows statistically significant increases in 2-NBDG fluorescence at all hypoxic time

points compared to the normoxic (0 h) cells. Cycling induces significant changes after 3 h for PANC-1 and 6 h for Caco-2 (Figure 7(B)).

Time course of changes in ALDH activity under hypoxia.

The ALDH activity was screened under both static and cycling hypoxia conditions using the BAAA fluorescent probe using fluorescence microscopy. The results show that ALDH activity increases over 24 h in PANC-1 cells (Figure S5). Cycling hypoxia leads to increased activity compared to static hypoxia.

To confirm our microscopy results, BAAA-treated cells were also examined by flow cytometry. Control experiments treated cells with ALDH-inhibiting reagent DEAB to establish the detection gates (Figure S6). The normoxic control indicated 3.93% of PANC-1 cells were positive for ALDH activity. Under static hypoxia, this increased over time to a maximum of 8.81% of the cells after 24 h (Figure S6). For cells exposed to cycling hypoxia, the results are shown in Figure 8. The normoxia control on the cycling plate shows a background level of 2.66% of cells staining positive for ALDH activity that increases over time to 33.0% at 24 h. On the same plate, 8.23% of cells exposed to 24 h of static hypoxia tested positive for ALDH activity.

DISCUSSION

Our laboratory[2] and others[22–26] have presented designs to control gas delivery to multiwell plates. This enables the evaluation of oxygen as controllable variable in high-throughput screening studies. However, none of these devices provided a facile method to vary the exposure time of cells to altered gas atmospheres. This is important in the study of dynamic metabolic networks since cellular response will change over time. For example, earlier studies report that hypoxia initially showed increases in HIF-1α protein levels but, subsequently, these levels fall even when hypoxic conditions are maintained[3–6,8–13]. However, changes in *HIF-1A* mRNA[5] or transcriptional activity,[6] may not correlate with the temporal changes in protein levels. Therefore, there is a need to provide a simplified method to screen the time dependence of cellular responses to changing oxygen conditions. The device described in this report is a modification of our earlier design[2] and utilizes a novel flow-encoded switching method so that a single plate can be used to follow the kinetics of protein or metabolic activity under static or cycling hypoxia. The results show that flow-encoded switching works well in delivering either one of two input gases to channels below each row in a permeable-bottom plate resulting in pericellular pO_2 levels of 1 or 137 mmHg. This plate design consumes lower gas volumes and is capable of providing rapid cycling patterns compared to flushing of hypoxia chambers. In addition, most hypoxia studies use standard low-permeability culture dishes and alter media oxygen content through changes in gas atmospheres. That approach can result in pericellular pO_2 levels that can change over time due cellular consumption and oxygen diffusion limitations.[27–29] Permeable bottom cell plates address this problem and thereby assure cells are exposed to a known, uniform gas atmosphere[30] and are being utilized to an increasing extent in hypoxia studies.[25,26,29,31] Unfortunately, many hypoxia studies do not report whether permeable bottom plates are used and few report on actual pO_2 levels in a plate. This new device design provides known

and uniform pericellular pO_2 levels throughout the experimental time course and is ideal for screening the time course of molecular changes induced in cultured cells upon exposure to static or cycling hypoxic conditions. Even with measured pO_2 ~ 1 mmHg in the wells for up to 24 h, cells remained viable.

Using these plates as a screening device, immunohistochemistry is a facile method to rapidly and qualitatively evaluate protein expression. In this study, we show that HIF-1α levels steadily increase over the 24 h study. This is in contrast to a number of reports that indicate HIF-1α levels peak at ≤12 h upon exposure to hypoxia.[3–9,12,13] The differences may be due to the higher sensitivity for detecting HIF-1α protein by Western blotting in the prior studies.

In comparison to cells exposed to static levels of hypoxia, both cell lines showed increased staining of HIF-1α in cells exposed to 30 min cycles of hypoxia-reoxygenation at each time point. The 30 min cycling period was chosen as an average dominant period found in *in vivo* tumors.[32]. Previous studies also noted increased HIF-1α protein levels in cells exposed to cycling compared to static hypoxia.[33,34]

Glucose uptake is due, in part to increase in expression of the GLUT-1 protein which is under transcriptional control of HIF-1α.[14] Activity of GLUT-1 or other glucose transporters can be screened using the fluorescent 2-deoxyglucose analog, 2-NBDG.[21] Glucose uptake increased in both cell lines over 24 h exposure to static hypoxia with greater increases in uptake with cycling hypoxia. An earlier study followed the time course of hypoxia-induced changes in the *GLUT1* gene in Caco-2 cells and initially found lower levels at 3 h than higher at 6 h compared to normoxia controls.[6] GLUT-1 protein levels were not measured in that study and our measure of total functional uptake activity may represent the activity of more than one glucose transporter isoform.

Hypoxia, through HIF-1α activation, can also induce stem-cell like characteristics in cells characterized by molecular changes that include increased ALDH activity.[15] Our data shows that ALDH activity increased over time and cycling hypoxia again showed higher levels of activity compared to static hypoxia. Earlier studies also demonstrated increased BAAA-detected ALDH activity upon exposure to hypoxia.[35–38] Cycling, as compared to static hypoxia is also known to increase stem-like properties in cells.[39,40]

CONCLUSION

These studies show that flow-encoding, paired with a single permeable-bottom plate can be used to easily assess the kinetics of molecular changes in hypoxia-related processes in cultured cells.

Supplementary Material

Refer to Web version on PubMed Central for supplementary material.

ACKNOWLEDGMENT

This work was supported by NIH Grant R21CA202804.

REFERENCES

(1). Vaupel P; Mayer A Hypoxia in tumors: pathogenesis-related classification, characterization of hypoxia subtypes, and associated biological and clinical implications Adv. Exp. Med. Biol 2014, 812, 19–24. [PubMed: 24729210]

(2). Yao M; Sattler T; Rabbani ZN; Pulliam T; Walker G; Gamcsik MP Mixing and delivery of multiple controlled oxygen environments to a single multiwell culture plate. Am. J. Physiol. Cell Physiol 2018, 315, C766–C775. [PubMed: 30183322]

(3). Holmquist-Mengelbier L; Fredlund E; Lofstedt T; Noguera R; Navarro S; Nilsson H; Pietras A; Vallon-Christersson J; Borg A; Gradin K; Poellinger L; Pahlman S Recruitment of HIF-1alpha and HIF-2alpha to common target genes is differentially regulated in neuroblastoma: HIF-2alpha promotes an aggressive phenotype Cancer Cell 2006, 10, 413–423. [PubMed: 17097563]

(4). Koh MY; Lemos R Jr.; Liu X; Powis G The hypoxia-associated factor switches cells from HIF-1alpha- to HIF-2alpha-dependent signaling promoting stem cell characteristics, aggressive tumor growth and invasion Cancer Res 2011, 71, 4015–4027. [PubMed: 21512133]

(5). Jiang Y; Zhu Y; Wang X; Gong J; Hu C; Guo B; Zhu B; Li Y Temporal regulation of HIF-1 and NF-kappaB in hypoxic hepatocarcinoma cells Oncotarget 2015, 6, 9409–9419. [PubMed: 25823824]

(6). Nguyen LK; Cavadas MA; Scholz CC; Fitzpatrick SF; Bruning U; Cummins EP; Tambuwala MM; Manresa MC; Kholodenko BN; Taylor CT; Cheong A A dynamic model of the hypoxia-inducible factor 1alpha (HIF-1alpha) network J. Cell. Sci 2013, 126, 1454–1463. [PubMed: 23390316]

(7). Jung DB; Lee HJ; Jeong SJ; Lee HJ; Lee EO; Kim YC; Ahn KS; Chen CY; Kim SH Rhapontigenin inhibited hypoxia inducible factor 1 alpha accumulation and angiogenesis in hypoxic PC-3 prostate cancer cells Biol. Pharm. Bull 2011, 34, 850–855. [PubMed: 21628883]

(8). Bae KM; Dai Y; Vieweg J; Siemann DW Hypoxia regulates SOX2 expression to promote prostate cancer cell invasion and sphere formation Am. J. Cancer Res 2016, 6, 1078–1088. [PubMed: 27294000]

(9). Botlagunta M; Krishnamachary B; Vesuna F; Winnard PT Jr.; Bol GM; Patel AH; Raman V Expression of DDX3 is directly modulated by hypoxia inducible factor-1 alpha in breast epithelial cells PLoS ONE 2011, 6, e17563. [PubMed: 21448281]

(10). Holmquist L; Jogi A; Pahlman S Phenotypic persistence after reoxygenation of hypoxic neuroblastoma cells. Int. J. Cancer 2005, 116, 218–225. [PubMed: 15800931]

(11). Jewell UR; Kvietikova I; Scheid A; Bauer C; Wenger RH; Gassmann M Induction of HIF-1alpha in response to hypoxia is instantaneous FASEB J 2001, 15, 1312–1314. [PubMed: 11344124]

(12). Kim DH; Sung B; Kim JA; Kang YJ; Hwang SY; Hwang NL; Suh H; Choi YH; Im E; Chung HY; Kim ND HS-1793, a resveratrol analogue, downregulates the expression of hypoxia-induced HIF-1 and VEGF and inhibits tumor growth of human breast cancer cells in a nude mouse xenograft model Int. J. Oncol 2017, 51, 715–723. [PubMed: 28656256]

(13). Vordermark D; Katzer A; Baier K; Kraft P; Flentje M Cell type-specific association of hypoxia-inducible factor-1 alpha (HIF-1 alpha) protein accumulation and radiobiologic tumor hypoxia Int. J. Radiat. Oncol. Biol. Phys 2004, 58, 1242–1250. [PubMed: 15001269]

(14). Muz B; de la Puente P; Azab F; Azab AK The role of hypoxia in cancer progression, angiogenesis, metastasis, an resistance to therapy. Hypoxia 2015, 3, 83–92. [PubMed: 27774485]

(15). Semenza GL The Hypoxic Tumor Microenvironment: A Driving Force for Breast Cancer Progression Biochim. Biophys. Acta 2016, 1863, 382–391. [PubMed: 26079100]

(16). Schneider CA; Rasband WS; Elcieri KW NIH Image to ImageJ: 25 years of image analysis. Nature Methods 2012, 9, 671–675. [PubMed: 22930834]

(17). McCloy RA; Rogers S; Caldon CE; Lorca T; Castro A; Burgess A Partial inhibition of Cdk1 in G 2 phase overrides the SAC and decouples mitotic events Cell Cycle 2014, 13, 1400–1412. [PubMed: 24626186]

(18). PreSens. PreSens Precision Sensing

(19). Wagner BA; Venkataraman S; Buettner GR The Rate of Oxygen Utilization by Cells Free Radic. Biol. Med 2011, 51, 700–712. [PubMed: 21664270]

(20). King KR; Wang S; Jayaraman A; Yarmush ML; Toner M Microfluidic flow-encoded switching for parallel control of dynamic cellular microenvironments Lab Chip 2008, 8, 107–116. [PubMed: 18094768]

(21). Millon SR; Ostrander JH; Brown JQ; Raheja A; Seewaldt VL; Rmanujam N Uptake of 2-NBDG as a method to monitor therapy response in breast cancer cell lines. Breast Cancer Res. Treat 2011, 126, 55–62. [PubMed: 20390344]

(22). Brennan MD; Rexius-Hall ML; Eddington DTA 3D-Printed Oxygen Control Insert for a 24-Well Plate PLoS ONE 2015, 10, e0137631. [PubMed: 26360882]

(23). Oppegard SC; Nam KH; Carr JR; Skaalure SC; Eddington DT Modulating temporal and spatial oxygenation over adherent cellular cultures. PLoS ONE 2009, 4, e6891. [PubMed: 19727397]

(24). Domansky K; Inman W; Serdy J; Dash A; Lim MH; Griffith LG Perfused multiwell plate for 3D liver tissue engineering Lab Chip 2010, 10, 51–58. [PubMed: 20024050]

(25). Minoves M; Morand J; Perriot F; Chatard M; Gonthier B; Lemarie E; Menut JB; Polak J; Pepin JL; Godin-Ribuot D; Briancon-Marjollet A An innovative intermittent hypoxia model for cell cultures allowing fast Po2 oscillations with minimal gas consumption Am. J. Physiol. Cell. Physiol 2017, 313, C460–c468. [PubMed: 28747336]

(26). Polak J; Studer-Rabeler K; McHugh H; Hussain MA; Shimoda LA System for exposing cultured cells to intermittent hypoxia utilizing gas permeable cultureware Gen. Physiol. Biophys 2015, 34, 235–247. [PubMed: 25816360]

(27). Metzen E; Wolff M; Fandrey J; Jelkmann W Pericellular PO2 and O2 consumption in monolayer cell cultures. Respir. Physiol 1995, 100, 101–106. [PubMed: 7624611]

(28). Pettersen EO; Larsen LH; Ramsing NB; Ebbesen P Pericellular oxygen depletion during ordinary tissue culturing, measured with oxygen microsensors Cell Prolif 2005, 38, 257–267. [PubMed: 16098184]

(29). Place TL; Domann FE; Case AJ Limitations of oxygen delivery to cells in culture: An underappreciated problem in basic and translational research Free Radic. Biol. Med 2017, 113, 311–322. [PubMed: 29032224]

(30). Jensen MD; Wallach DFH; Sherwood P Diffusion in tissue cultures on gas-permeable and impermeable supports. J. Theoret. Biol 1976, 56, 443–458. [PubMed: 5633]

(31). Zeitouni NE; Fandrey J; Naim HY; von Kockritz-Blickwede M Measuring oxygen levels in Caco-2 cultures Hypoxia (Auckl) 2015, 3, 53–66. [PubMed: 27774482]

(32). Dewhirst MW Relationships between cycling hypoxia, HIF-1, angiogenesis and oxidative stress. Radiat. Res 2009, 172, 653–665. [PubMed: 19929412]

(33). Liu H; Jiang F; Jia X; Lan J; Guo H; Li E; Yan A; Wang Y Cycling hypoxia affects cell invasion and proliferation through direct regulation of claudin1 / claudin7 expression, and indirect regulation of P18 through claudin7 Oncotarget 2017, 8, 10298–10311. [PubMed: 28055967]

(34). Chen WL; Wang CC; Lin YJ; Wu CP; Hsieh CH Cycling hypoxia induces chemoresistance through the activation of reactive oxygen species-mediated B-cell lymphoma extra-long pathway in glioblastoma multiforme J. Transl. Med 2015, 13, 389. [PubMed: 26711814]

(35). An SM; Lei HM; Ding XP; Sun F; Zhang C; Tang YB; Chen HZ; Shen Y; Zhu L Interleukin-6 identified as an important factor in hypoxia- and aldehyde dehydrogenase-based gefitinib adaptive resistance in non-small cell lung cancer cells Oncol. Lett 2017, 14, 3445–3454. [PubMed: 28927099]

(36). Iriondo O; Rabano M; Domenici G; Carlevaris O; Lopez-Ruiz JA; Zabalza I; Berra E; Vivanco M Distinct breast cancer stem/progenitor cell populations require either HIF1alpha or loss of PHD3 to expand under hypoxic conditions Oncotarget 2015, 6, 31721–31739. [PubMed: 26372732]

(37). Shiraishi A; Tachi K; Essid N; Tsuboi I; Nagano M; Kato T; Yamashita T; Bando H; Hara H; Ohneda O Hypoxia promotes the phenotypic change of aldehyde dehydrogenase activity of breast cancer stem cells Cancer Sci 2017, 108, 362–372. [PubMed: 28012234]

(38). Soehngen E; Schaefer A; Koeritzer J; Huelsmeyer V; Zimmer C; Ringel F; Gempt J; Schlegel J Hypoxia upregulates aldehyde dehydrogenase isoform 1 (ALDH1) expression and induces functional stem cell characteristics in human glioblastoma cells Brain Tumor Pathol 2014, 31, 247–256. [PubMed: 24197864]

(39). Alhawarat FM; Hammad HM; Hijjawi MS; Sharab AS; Abuarqoub DA; Al Shhab MA; Zihlif MA The effect of cycling hypoxia on MCF-7 cancer stem cells and the impact of their microenvironment on angiogenesis using human umbilical vein endothelial cells (HUVECs) as a model PeerJ 2019, 7, e5990. [PubMed: 30729067]

(40). Louie E; Nik S; Chen J; Schmidt M; Song B; Pacson C; Chen XF; Park S; Ju J; Chen EI Identification of a stem-like cell population by exposing metastatic breast cancer cell lines to repetitive cycles of hypoxia and reoxygenation. Breast Cancer Res 2010, 12, R94. [PubMed: 21067584]

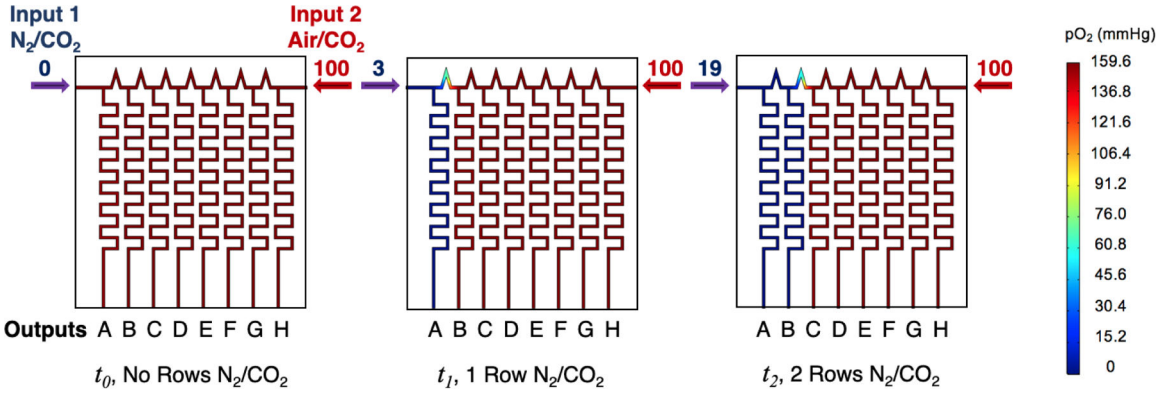

Figure 1.

COMSOL modeling of pO_2 content in flow-encoding manifold at different flow-rates of Input 1 Gas 95% N_2 /5% CO_2 and Input 2 Gas 95% Air/5% CO_2 at an initial time point, t_0, and arbitrary time points t_1,t_2. At t_1, the N_2/CO_2 flow rate is increased to 3 mL/min, which causes output A to become hypoxic. At t_2, the flow rate is further increased to 19 mL/min, causing outputs A and B to become hypoxic. The flow rates of the two gases are given above the blue and red arrows in each figure. The heat maps of content show sequential switching of output gas channels of each row A-B from air/CO_2 to N_2/CO_2 at each time point.

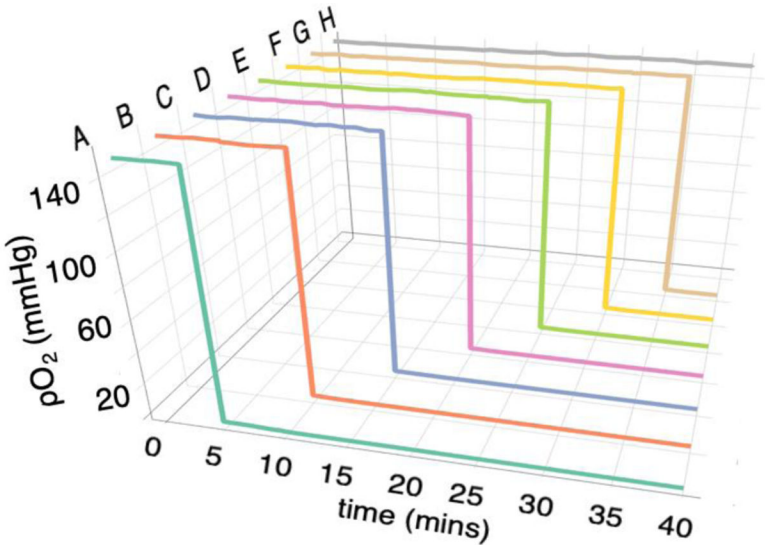

Figure 2.

Measured gas outputs from the manifold with flow-encoded switching occurring every 5 min at the flow-rates given in Table 1. Row H remains at pO_2 = 151 mmHg.

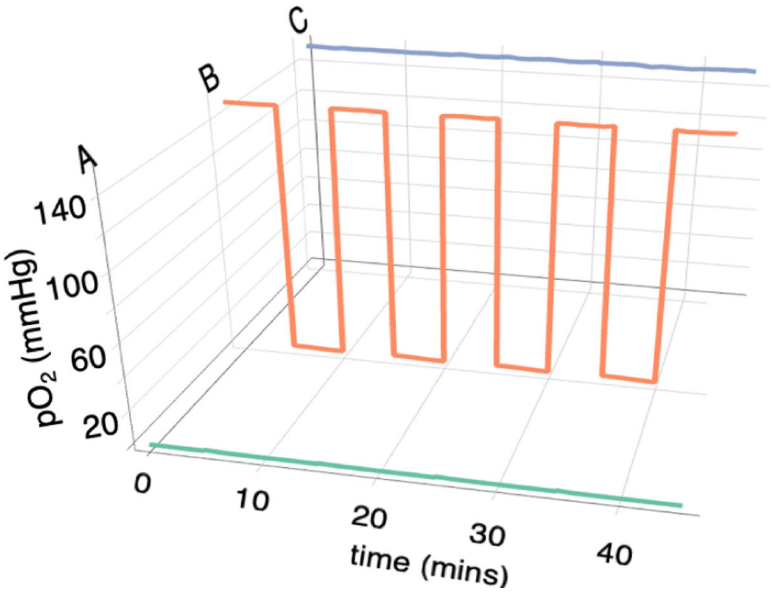

Figure 3.

Measured pO_2 levels at the manifold outputs when the input flow rates were switched every 5 min and designed to maintain output to Row A at constant N_2, output B was cycled between N_2 and air and the outputs to C-H were held at constant air. Only the outputs to rows A - C are shown.

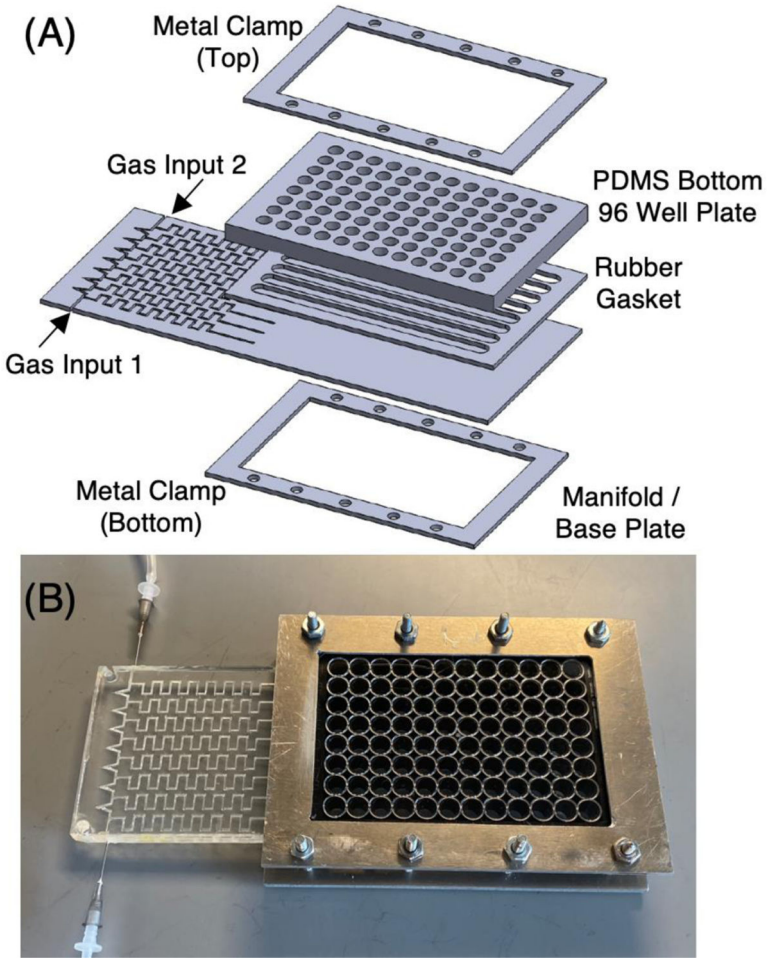

Figure 4.

(A) A diagram of the device showing the 96-well plate, the gasket below the plate and the gas manifold designed to deliver gas mixtures to channels below each row of wells in the plate. (B) A view of the assembled device.

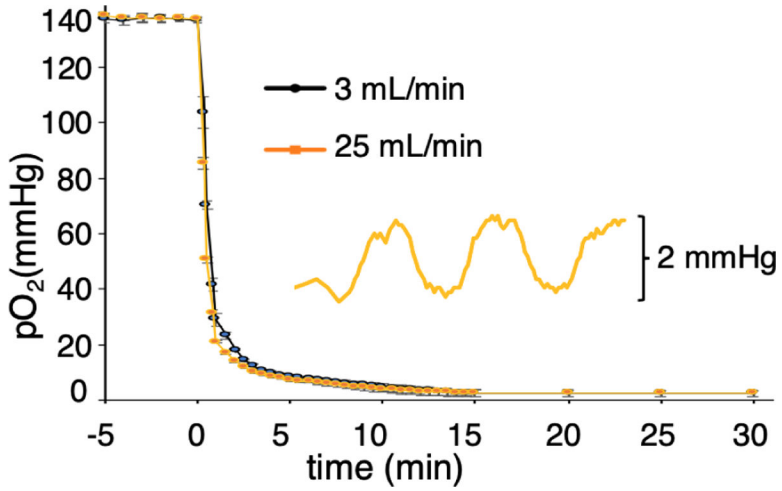

Figure 5.

Time course of the O_2 sensor response in a water-filled well at 37 °C as gas input switches from air/CO_2 to N_2/CO_2. The responses shown are for gas flow rates of 3mL/min (black line) and 25 mL/min (orange line). The inset shows the response of the sensor in the well when gas is cycled between N_2/CO_2 and 1% air/CO_2 (pO_2=1.6 mmHg) every 5 min.

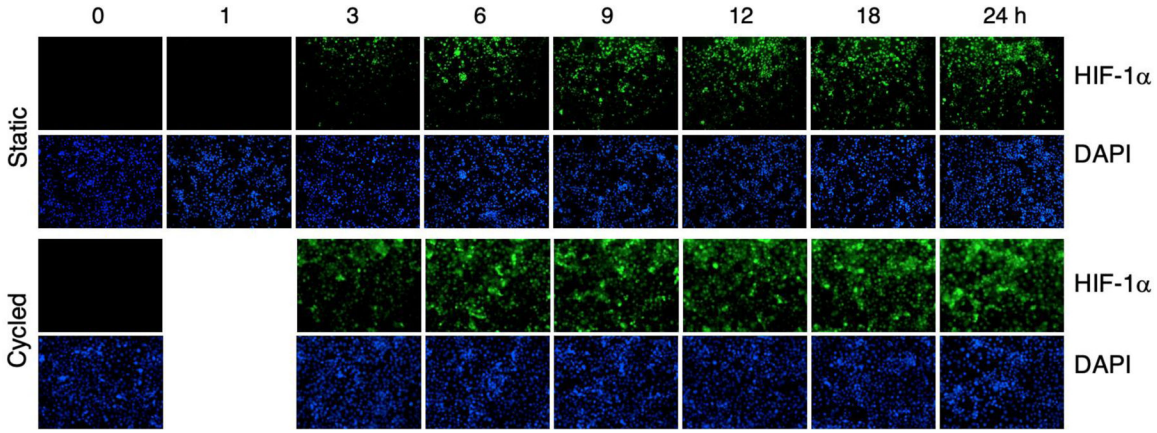

Figure 6.

Histochemistry of HIF-1α in PANC-1 cells exposed to static hypoxia (top series) between 0 and 24 h. The bottom series shows cell response to cycles of 30 min of hypoxia followed by 30 min of air for periods between 0 and 24 h. The top row in each series shows HIF-1α staining whereas the bottom rows show DAPI staining of cell nuclei.

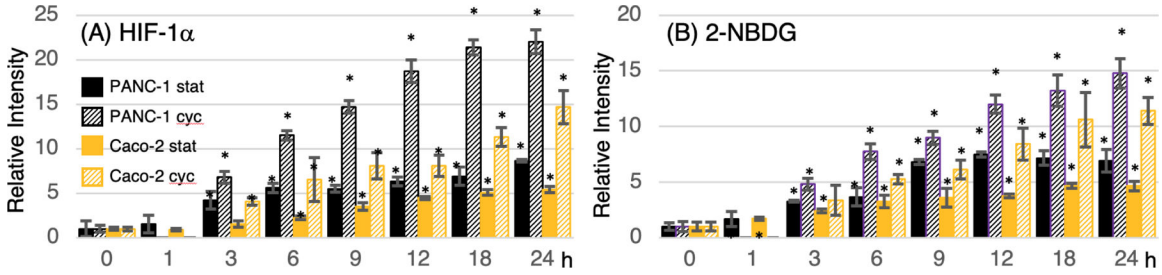

Figure 7:

Quantification of fluorescent micrographs for (A) HIF-1α immunohistochemistry and (B) 2-NBDG uptake in PANC-1 cells and Caco-2 cells under static (stat) or cycling (cyc) hypoxia for periods ranging between 1 and 24 h (static) or 3 – 24 h (cycling). The key to the bar plots in both figures is shown in (A). The asterisks denote statistical significance ($P < 0.05$) for hypoxic cells compared to the normoxic control (0 h).

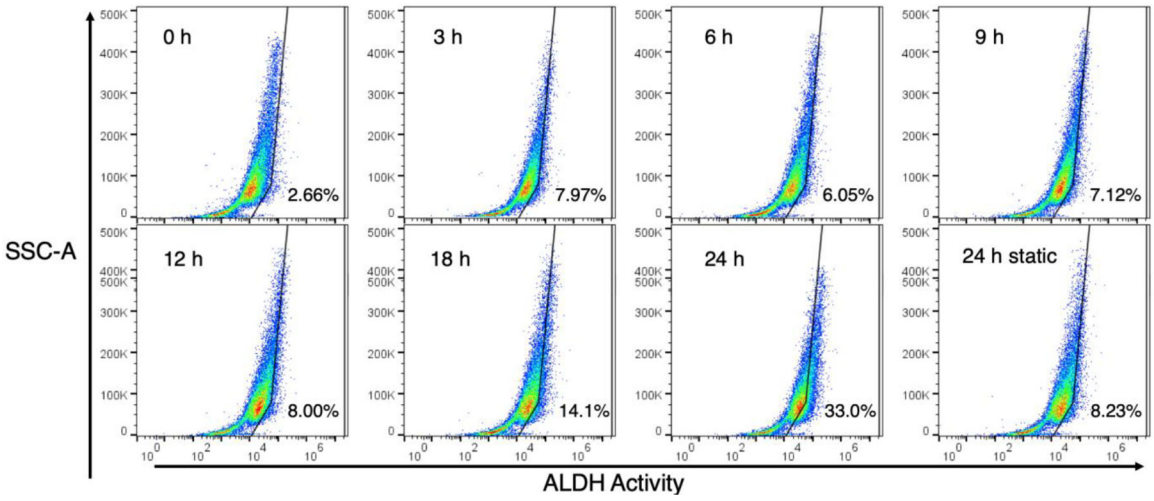

Figure 8.

Flow cytometry results for aldehyde dehydrogenase activity in PANC-1 cells exposed to cycling hypoxia. The percent of cells staining positive for ALDH activity are shown in the lower right of each plot.

Table 1.

Predicted pO_2 Levels From Input Flow Rates

Flow Rates (ml/min)			**Predicted pO_2 Outputs (mmHg)**							
time	**Input1**	**Input 2**	**A**	**B**	**C**	**D**	**E**	**F**	**G**	**H**
t_0	0	100	151.0	151.0	151.0	151.0	151.0	151.0	151.0	151.0
t_1	3	100	0.6	149.8	151.0	151.0	151.0	151.0	151.0	151.0
t_2	19	100	0	0.5	149.9	151.0	151.0	151.0	151.0	151.0
t_3	49	100	0	0	0.5	150.6	151.0	151.0	151.0	151.0
t_4	100	100	0	0	0	0	150.6	151.0	151.0	151.0
t_5	100	49	0	0	0	0	0.2	150.1	151.0	151.0
t_6	100	19	0	0	0	0	0	0.5	149.9	151.0
t_7	100	3	0	0	0	0	0	0	0.6	149.8